PROCEEDINGS OF SCIENCE

KamLAND

I. Shimizu[*†]
Research Center for Neutrino Science, Tohoku University, Aramaki Aoba, Aoba, Sendai, Miyagi 980-8578, Japan
E-mail: shimizu@awa.tohoku.ac.jp

KamLAND reports on a precise measurement of neutrino oscillation parameters with reactor $\overline{\nu}_e$, and an estimate of geo $\overline{\nu}_e$ flux including the period of the recent long-term shutdown of Japanese nuclear reactors. KamLAND-Zen reports on a preliminary search for neutrinoless double-beta decay with ^{136}Xe based on 114.8 live-days after the purification of the xenon loaded liquid scintillator. By combining the KamLAND-Zen pre- and post-purification data, we obtain a preliminary lower limit on the $0\nu\beta\beta$ decay half-life of $T^{0\nu}_{1/2} > 2.6 \times 10^{25}$ yr at 90% C.L. In this article, the latest results and future prospects of KamLAND and KamLAND-Zen are reviewed.

XVI International Workshop on Neutrino Telescopes,
2-6 March 2015
Palazzo Franchetti - Istituto Veneto, Venice, Italy

[*]Speaker.
[†]On behalf of the KamLAND and KamLAND-Zen Collaboration.

PoS(NEUTEL2015)048

1. Introduction

KamLAND is the largest liquid scintillator (LS) detector ever constructed, which was designed primarily to detect anti-neutrinos from distant nuclear reactors. The KamLAND data showed a clear oscillatory shape in the survival probability of reactor anti-neutrinos, resulting in the most precise measurement of the neutrino oscillation parameter Δm^2_{21}. KamLAND is also capable to detecting the geologically-produced anti-neutrinos (geo $\overline{\nu}_e$'s) from decays of primordial radioactivities, ^{238}U and ^{232}Th, which provide key information to understand the Earth's interior. We showed the first experimental study of geo $\overline{\nu}_e$'s [1], and later, the radiogenic heat production was measured to constrain Earth's compositional models [2, 3]. Meanwhile, we found KamLAND provides the ultra-low-background environment to realize the neutrinoless double-beta decay search with high sensitivity if we use enriched xenon-loaded LS contained in a clean mini-balloon. An initial $0\nu\beta\beta$ decay search based on an initial 213.4 days of measurement (denoted as "phase-1") provides a lower limit on the $0\nu\beta\beta$ decay half-life of $T^{0\nu}_{1/2} > 1.9 \times 10^{25}$ yr at 90% C.L. [4]. The $0\nu\beta\beta$ decay search sensitivity was limited by an identified background peak from ^{110m}Ag, so we embarked on the purification campaign to improve the sensitivity. We presented a preliminary result based on 114.8 days of measurement (denoted as "phase-2") after the purification [5]. This article reviews the latest results and future prospects of KamLAND and KamLAND-Zen.

2. Detector

The KamLAND detector is located in Kamioka mine at a depth of 1,000 m. The thick rock overburden suppresses the cosmic-ray muon flux by about 5 orders of magnitude. The primary target of $\overline{\nu}_e$ detection is 1,000 ton LS contained in the outer balloon, and the scintillation light is

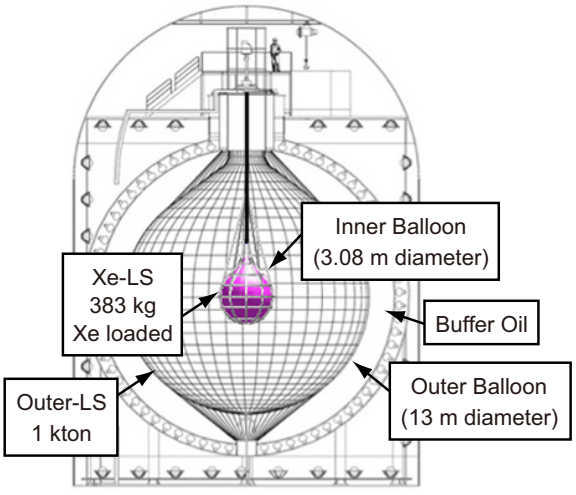

Figure 1: Schematic view of the KamLAND / KamLAND-Zen detector. The outer-LS is the neutrino interaction target, and the Xe-LS contains the double-beta decay target, 320 kg of ^{136}Xe enriched Xe in phase-1 and 383 kg in phase-2.

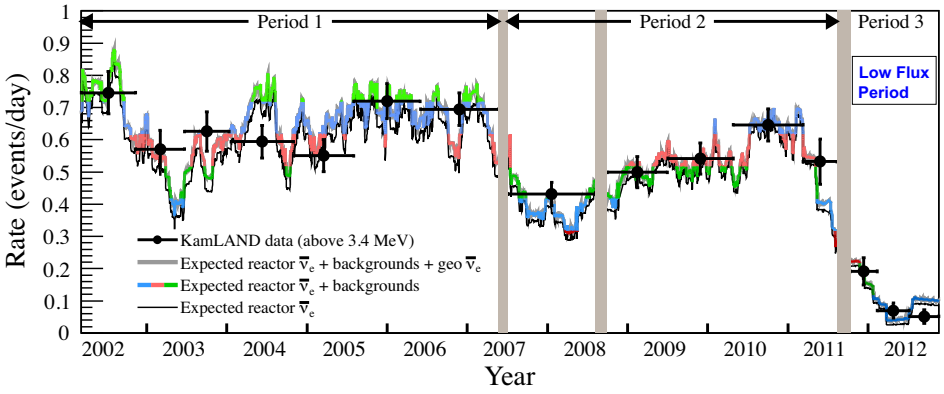

Figure 2: Time variation of expected and observed rates of $\overline{\nu}_e$'s with energies above 3.4 MeV in KamLAND data over 10 years [3]. The vertical grey bands indicate deadtime during the liquid scintillator purification and the detector modification.

viewed by surrounding 1,879 PMTs. A buffer oil between the outer balloon and an 18-m-diameter spherical stainless steel vessel shields the LS from external gamma-rays. Since September 2011, we started the KamLAND-Zen experiment by the installation of $\beta\beta$ source, 13 tons of Xe-loaded LS in a 3.08-m-diameter inner balloon at the center of the detector [4]. The detector is illustrated schematically in Fig. 1.

3. KamLAND result

The anti-neutrino analyses presented here are based on Ref. [3]. The data set is divided into three periods: Period 1 (March 2002 - May 2007); before the LS purification, Period 2 (May 2007 - August 2011); during and after the LS purification, and Period 3 (October 2011 - November 2012); after the KamLAND-Zen start. Recent long-term shutdown of Japanese reactors after 2011 reduce the $\overline{\nu}_e$ rate as illustrated in Fig. 2, and allows us the "Reactor on-off" study for neutrino oscillations and geo $\overline{\nu}_e$'s below 3.4 MeV in neutrino energy.

The reactor neutrino flux can be calculated based on the reactor operation records, and the comparison between the calculated oscillated $\overline{\nu}_e$ spectra and the observed spectra gives estimates of the neutrino oscillation parameters and geo $\overline{\nu}_e$ fluxes. We constructed an unbinned maximum-likelihood method incorporating the event rate and the prompt energy spectrum shape, including their time variations in the range $0.9\,\mathrm{MeV} < E_\mathrm{p} < 8.5\,\mathrm{MeV}$. The χ^2 is defined by

$$\begin{aligned}\chi^2 = {} & \chi^2_\mathrm{rate}(\theta_{12},\theta_{13},\Delta m^2_{21},N_\mathrm{BG},N^\mathrm{geo}_\mathrm{U,Th},\alpha) \\ & -2\ln L_\mathrm{shape}(\theta_{12},\theta_{13},\Delta m^2_{21},N_\mathrm{BG},N^\mathrm{geo}_\mathrm{U,Th},\alpha) \\ & +\chi^2_\mathrm{BG}(N_\mathrm{BG})+\chi^2_\mathrm{syst}(\alpha) \\ & +\chi^2_\mathrm{osci}(\theta_{12},\theta_{13},\Delta m^2_{21})\,. \end{aligned} \tag{3.1}$$

The first and second term represents the χ^2 contribution for the total event rate and the time-varying prompt energy spectrum shape, respectively. The last three terms indicate penalty terms

for backgrounds, systematic uncertainties, and oscillation parameters. For the geo $\overline{\nu}_e$ measurement, the largest background comes from the reactor $\overline{\nu}_e$ which is mainly constrained by the higher energy data and the solar neutrino oscillation data.

Based on the χ^2 fit to the entire data set, the oscillation parameters are estimated. Figure 3 shows the prompt energy spectra of $\overline{\nu}_e$ candidate events for each period. For the three-flavor KamLAND-only analysis ($\chi^2_{\rm osci} = 0$), the oscillation parameters are fitted to be $\Delta m^2_{21} = 7.54^{+0.19}_{-0.18} \times 10^{-5}\,{\rm eV}^2$, $\tan^2\theta_{12} = 0.481^{+0.092}_{-0.080}$, and $\sin^2\theta_{13} = 0.010^{+0.033}_{-0.034}$. Assuming *CPT* invariance, the oscillation parameters from a combined analysis including constraints from solar neutrino experiments are fitted to be $\tan^2\theta_{12} = 0.437^{+0.029}_{-0.026}$, $\Delta m^2_{21} = 7.53^{+0.19}_{-0.18} \times 10^{-5}\,{\rm eV}^2$, and $\sin^2\theta_{13} = 0.023^{+0.015}_{-0.015}$. Including also constraints on θ_{13} from accelerator and short-baseline reactor neutrino experiments, we obtains $\tan^2\theta_{12} = 0.436^{+0.029}_{-0.025}$, $\Delta m^2_{21} = 7.53^{+0.18}_{-0.18} \times 10^{-5}\,{\rm eV}^2$, and $\sin^2\theta_{13} = 0.023^{+0.002}_{-0.002}$.

The determination of oscillation parameters made it possible to study the abundance of U and Th producing radiogenic heat in the Earth's interior based on the $\overline{\nu}_e$ flux measurement. Assuming the Th/U mass ratio of 3.9 based on the geochemical model [6], the total number of U and Th geo $\overline{\nu}_e$ events is fitted to be 116^{+28}_{-27}, which corresponds to an oscillated $\overline{\nu}_e$ flux of $3.4^{+0.8}_{-0.8} \times 10^6\,{\rm cm}^{-2}{\rm s}^{-1}$ at the KamLAND location. The KamLAND data [3] tested three BSE compositional estimates of geo $\overline{\nu}_e$ flux at Kamioka and radiogenic heat from ^{238}U and ^{232}Th [7], as shown in Figure 4.

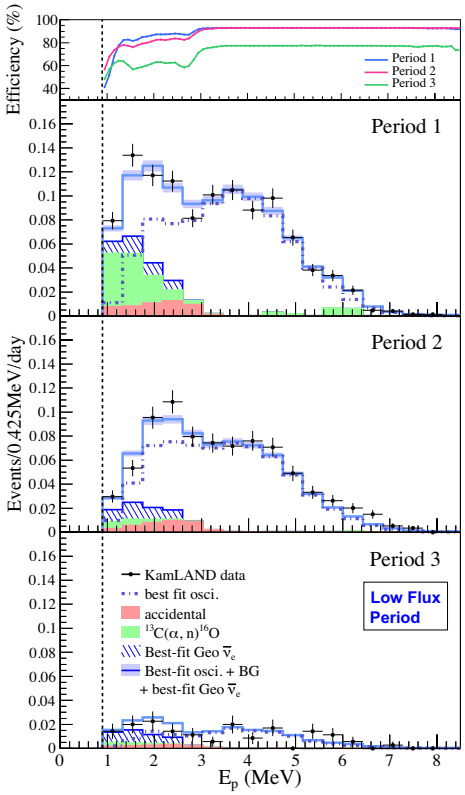

Figure 3: Prompt energy spectrum of $\overline{\nu}_e$ candidate events above the 0.9 MeV energy threshold (vertical dashed line) for each data taking period. The background, reactor and geo $\overline{\nu}_e$ contributions are the best-fit values from a KamLAND-only analysis without a penalty term for oscillation parameters. The top panel shows the energy-dependent selection efficiency curves for each period.

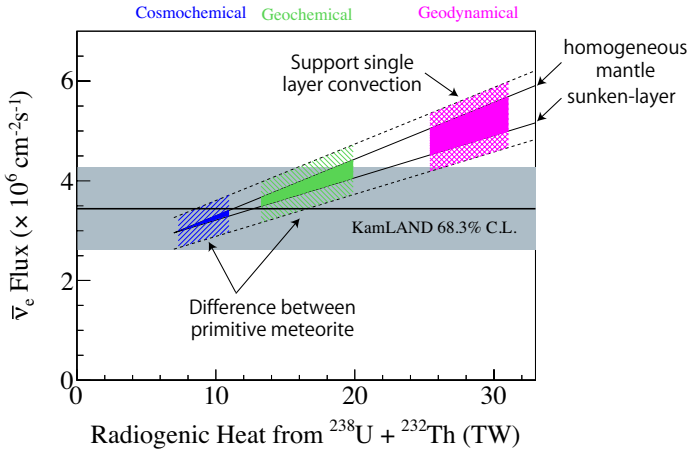

Figure 4: Three BSE compositional estimates of geo $\bar{\nu}_e$ flux and radiogenic heat from ^{238}U and ^{232}Th [3]. The colored shaded regions indicate the different mantle model predictions from cosmochemical, geochemical, and geodynamical estimates. The variations due to the radiochemical distributions are represented by the two solid lines with different slopes; the homogeneous and sunken-layer hypotheses. The uncertainties from the crustal contributions are indicated by the colored hatched regions.

The upper solid line indicates the estimate in the homogeneous mantle assumption and the crustal model based on [8]. Based on these assumptions, the measured geo $\bar{\nu}_e$ flux can be converted into a radiogenic heat of $11.2^{+7.9}_{-5.1}$ TW from U and Th. We found the radiogenic heat is smaller than the heat flow of 47 ± 2 TW from Earth's surface [9], indicating secular cooling of the Earth. The KamLAND data disfavors the geodynamical model with the homogeneous hypothesis at 89% C.L., but still consistent within $\sim 2\sigma$ C.L. Currently, cosmochemical and geochemical models based on different assumptions of the primitive meteorite are consistent with the data within $\sim 1\sigma$ C.L.

4. KamLAND-Zen result

Preliminary results for the double-beta decay analyses presented here are based on the phase-2 data, collected between December 11, 2013, and May 1, 2014, after the ^{110m}Ag background reduction [5]. The total livetime is 114.8 days. After the phase-1 data-taking, we made several efforts for further improvements: (i) the removal of radioactive impurities by Xe-LS purification; (ii) increasing the Xe concentration from (2.44 ± 0.01) wt% to (2.96 ± 0.01) wt%, indicating the $\beta\beta$ target increase relative to radioactive backgrounds; (iii) developing a spallation background rejection method for ^{10}C from muon-spallation; (iv) optimization of the volume selection to minimize the effect of the mini-balloon backgrounds.

The ^{136}Xe $2\nu\beta\beta$ decay rate is estimated from a fit to the energy spectrum of $\beta\beta$ candidates within the fiducial radius of 1.0 m in order to avoid a large ^{134}Cs/^{137}Cs background at the mini-balloon. The measured $2\nu\beta\beta$ decay half-life of ^{136}Xe is $T^{2\nu}_{1/2} = 2.32 \pm 0.05(\text{stat}) \pm 0.08(\text{syst}) \times 10^{21}$ yr. This is consistent with the previous result based on the phase-1 data, $T^{2\nu}_{1/2} = 2.30 \pm 0.02(\text{stat}) \pm 0.12(\text{syst}) \times 10^{21}$ yr [10].

The $0\nu\beta\beta$ decay rate is estimated by the fit to 2-dimensional spectra in energy-volume in the full 2-m-radius analysis volume. The volume is divided into radial-equal-volume bins, 20 bins in

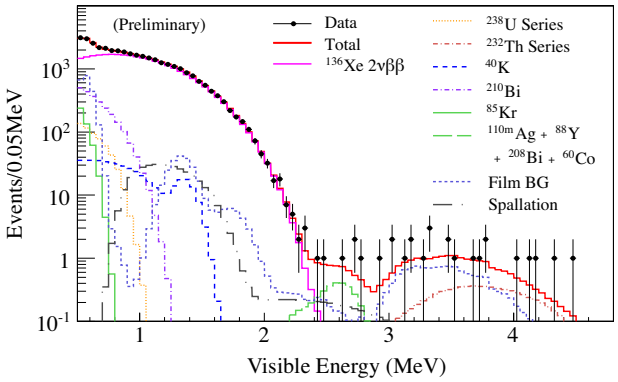

Figure 5: Preliminary energy spectrum of selected $\beta\beta$ candidates within 1.0 m fiducial radius is shown together with the best-fit backgrounds, with the $2\nu\beta\beta$ decay fit.

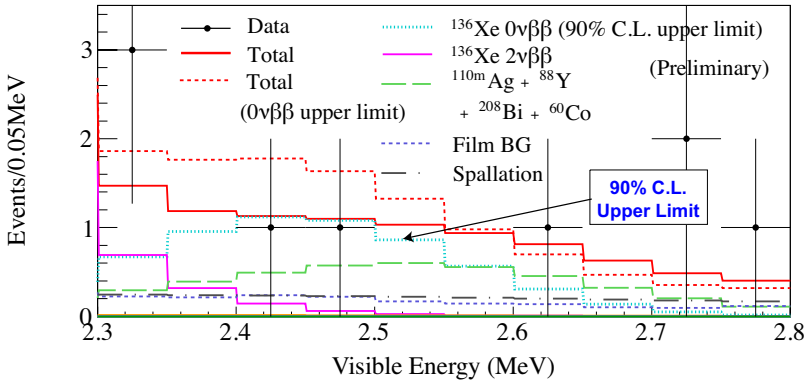

Figure 6: Preliminary energy spectrum of selected $\beta\beta$ candidates within the radius cut $R < 1.0$ m is shown together with the best-fit backgrounds and the 90% C.L. upper limit for $0\nu\beta\beta$ decays.

the upper and lower hemisphere each for signal-to-background optimization. The potential background contributions of ^{110m}Ag, ^{88}Y, ^{208}Bi, and ^{60}Co in the $0\nu\beta\beta$ region of interest are allowed to vary in the fit. We found no event excess over the background expectation. The 90% C.L upper limit on the ^{136}Xe $0\nu\beta\beta$ decay rate is < 17.0 (kton·day)$^{-1}$, in Xe-LS mass units. The $0\nu\beta\beta$ decay contribution corresponding to the 90% C.L. upper limit for the internal volume is shown in Fig. 6. Considering the Xe concentration in the Xe-LS, we obtain a limit on the ^{136}Xe $0\nu\beta\beta$ decay half-life of $T^{0\nu}_{1/2} > 1.3 \times 10^{25}$ yr (90% C.L.).

As shown in Fig. 7, the combined KamLAND-Zen result from the phase-1 [4] and phase-2 data gives a 90% C.L. lower limit of $T^{0\nu}_{1/2} > 2.6 \times 10^{25}$ yr. This limit is compared to the recent EXO-200 result, which tends to allow shorter half-life values, and gives a 90% C.L. lower limit of $T^{0\nu}_{1/2} > 1.1 \times 10^{25}$ yr [11]. Based on nuclear matrix elements (NMEs) from various (R)QRPA models [12], the combined KamLAND-Zen half-life limit can be converted to a 90% C.L. upper limit of $\langle m_{\beta\beta} \rangle < (140 - 280)$ meV.

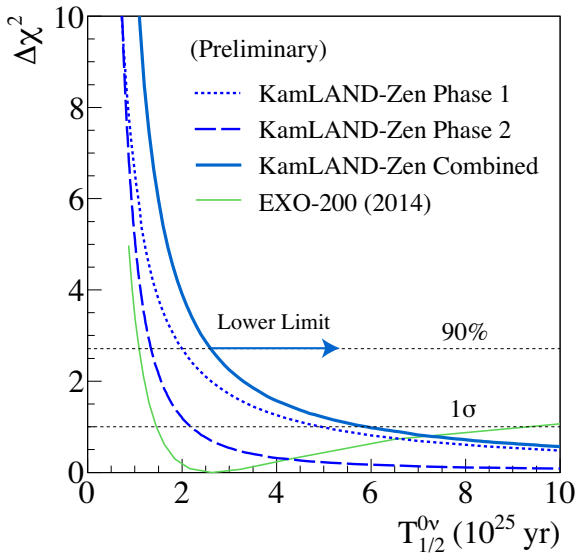

Figure 7: $\Delta\chi^2$-profile from the fit to the half-life of ^{136}Xe $0\nu\beta\beta$ decays in this work (phase-2), the previous work (phase-1), and the combined result (phase-1 + phase-2). The result from EXO-200 [11] is also shown for comparison.

5. Prospects

KamLAND anti-neutrino observation without Japanese reactor $\overline{\nu}_e$ flux continues even after KamLAND-Zen data-taking. It provides a chance of a rapid improvement of the geo $\overline{\nu}_e$ measurement accuracy. In addition, another geo $\overline{\nu}_e$ data by Borexino in Italy is also running [13], so the combined analysis of the multi-site measurements at different geological locations can be realized. If more multi-site data become available in the future, the combined analysis considering geological correlations will help the construction of a detail map of neutrino sources inside the Earth.

The $0\nu\beta\beta$ decay search sensitivity will steadily increase by accumulating additional low background data after the ^{110m}Ag reduction. Assuming the best-fit background rates in phase-2, the $T^{0\nu}_{1/2}$ sensitivity at 90% C.L. will reach 3×10^{25} yr within 2 years using the phase-2 data alone, see Fig. 8. We plan to rebuild the new mini-balloon to increase the Xe amount to about 700 kg and reduce the mini-balloon radioactivity by introducing a cleaner material for the balloon film. The next phase with those improvements will start in 2016. The expected sensitivities for phase-2 and next phase are shown in Fig. 8. In the next phase, a 2 year measurement yields the sensitivity of 2×10^{26} yr, which corresponds to $\langle m_{\beta\beta}\rangle = 50$ meV for the largest NME in the (R)QRPA models [12]. The next near-future $0\nu\beta\beta$ decay search milestone is to reach a sensitivity of $\langle m_{\beta\beta}\rangle \sim 20$ meV which covers the inverted neutrino mass hierarchy. A sensitivity covering the inverted hierarchy is projected to be achieved by "KamLAND2-Zen", which is a detector upgrade plan to have better energy resolution against the $2\nu\beta\beta$ background, by introducing light collective mirrors (1.8× light yield), new brighter LS (1.4× light yield), and high quantum efficiency PMTs (1.9× light yield). Owing to those improvements, the energy resolution is expected to be reduced from 4.0% to <2.5% at the Q-value of ^{136}Xe $\beta\beta$ decay. The Xe amount will be increased to 1,000 kg or more, then the target

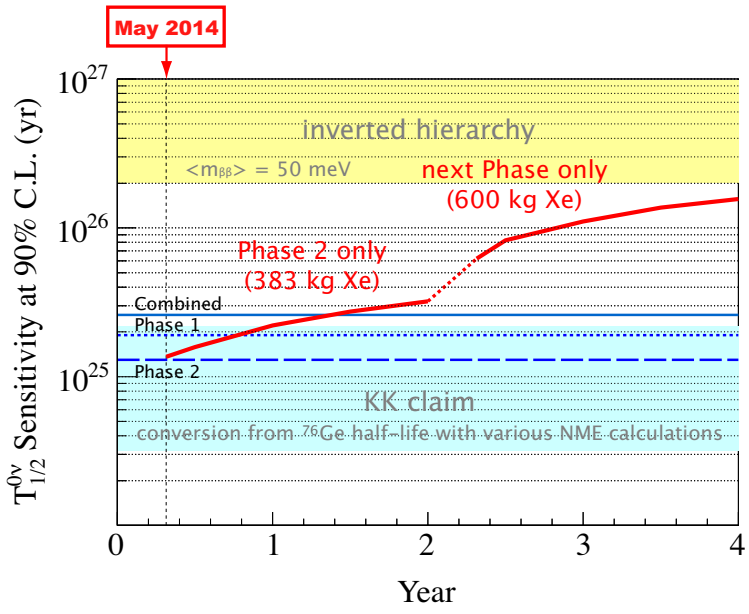

Figure 8: Expected $T^{0\nu}_{1/2}$ sensitivity at 90% C.L. in the near future for KamLAND-Zen. The red line at less than 2 years corresponds to phase-2 only, and the following red line is next phase only. The three horizontal lines indicate the lower $T^{0\nu}_{1/2}$ limits reported here (phase-2), the previous results (phase-1), and the combined result (phase-1 + phase-2).

sensitivity of 20 meV will be achieved in a 5 year measurement.

6. Summary

KamLAND performed a precise measurement of neutrino oscillation parameters with reactor $\overline{\nu}_e$, and provided a useful estimate of geo $\overline{\nu}_e$ flux to constrain the Earth models. Recent data with a low reactor $\overline{\nu}_e$ flux will improve the geo $\overline{\nu}_e$ flux accuracy. We also demonstrated the KamLAND-Zen ^{136}Xe $0\nu\beta\beta$ decay search was improved by the purification of the xenon loaded liquid scintillator. Several detector upgrades are planned for sensitivity enhancement in the future.

References

[1] T. Araki and et al., (KamLAND Collaboration), Nature **436**, 499 (2005).

[2] A. Gando and et al., (KamLAND Collaboration), Nature Geosci. **4**, 647 (2011).

[3] A. Gando and et al., (KamLAND Collaboration), Phys. Rev. D **88**, 033001 (2013).

[4] A. Gando *et al.*, (KamLAND-Zen Collaboration), Phys. Rev. Lett. **110**, 062502 (2013).

[5] K. Asakura *et al.*, (KamLAND-Zen Collaboration), arXiv:1409.0077 .

[6] W. F. McDonough and S.-s. Sun, Chem. Geol. **120**, 223 (1995).

[7] O. Šrámek *et al.*, Earth and Planet. Sci. Lett. **361**, 356 (2013).

[8] S. Enomoto, E. Ohtani, K. Inoue, and A. Suzuki, Earth and Planet. Sci. Lett. **258**, 147 (2007).

[9] J. H. Davies and D. R. Davies, Solid Earth **1**, 5 (2010).

[10] A. Gando *et al.*, (KamLAND-Zen Collaboration), Phys. Rev. C **86**, 021601 (2012).

[11] J. Albert *et al.*, (EXO Collaboration), Nature **510**, 229 (2014).

[12] A. Faessler, V. Rodin, and F. Šimkovic, J. of Phys. G **39**, 124006 (2012).

[13] G. Bellini and et al., (Borexino Collaboration), Phys. Lett. B **722**, 295 (2013).